Journal of Materials Chemistry A

REVIEW

View Article Online
View Journal | View Issue

Cite this: *J. Mater. Chem. A*, 2022, **10**, 15865

MBenes: progress, challenges and future

Bikun Zhang, [ab] Jian Zhou *[ab] and Zhimei Sun *[ab]

Received 30th April 2022
Accepted 29th June 2022

DOI: 10.1039/d2ta03482d

rsc.li/materials-a

The prevalence of MXenes, two-dimensional (2D) transition metal carbides/nitrides separated from layered MAX phases, has generated much interest in exploring 2D transition metal borides during the past decade. In 2017, we first reported a new family of 2D transition metal borides as analogues to MXenes and coined a catchy name for them, *MBenes*. Over the last five years, MBenes have gained more and more attentions in the fields of nanomaterials, physics and chemistry. The promising future of MBenes is foreseeable since they have exhibited many intriguing properties and been widely studied for energy storage and electrocatalysis applications. However, research on MBenes is still in its infancy, with many expected properties and applications awaiting to be explored. In this review, first we made a scientific classification of 2D transition metal borides and proposed an explicit definition of MBenes: a family of 2D transition metal borides with sandwich-like structures which are derived from layered MAB phases. Then we reviewed the progress of synthesis methods, properties and applications of MBenes for energy storage and electrocatalysis. Finally, the discussions on the existing problems in experimental synthesis and theoretical calculations along with the perspectives and prospects of MBenes were presented.

1 Introduction

The exfoliation of graphene from graphite in 2004 (ref. 1) brought two-dimensional (2D) materials into people's vision. Since then, attentions to 2D materials have increased rapidly and a variety of 2D materials keep emerging in an endless stream,[2] including hexagonal boron nitride (h-BN),[3] transition metal dichalcogenides (TMDs),[4] layered double hydroxides (LDHs),[5] black phosphorous (BP),[6] MXenes,[7] MBenes[8–10] and so on. MXenes have flourished over the past decade since the first preparation of $Ti_3C_2T_x$ by Gogotsi and Barsoum *et al.* in 2011.[7] MXenes are 2D transition metal carbides, nitrides and carbonitrides with the general formula of $M_{n+1}X_nT_x$ (n = 1–4), where M, X and T represent transition metal, carbon/nitrogen and surface terminations, respectively.[11] MXenes are derived from the corresponding MAX phases, $M_{n+1}AX_n$, which are

[a]*School of Materials Science and Engineering, Beihang University, Beijing 100191, China*
[b]*Center for Integrated Computational Materials Engineering, International Research Institute for Multidisciplinary Science, Beihang University, Beijing 100191, China*

Dr. Bikun Zhang obtained his Ph.D. from the School of Materials Science and Engineering, Beihang University in 2022, supervised by Prof. Zhimei Sun. His research interests focus on the first-principles calculations of two-dimensional materials for catalysis. Dr Zhang has published 7 peer-reviewed SCI papers on international journals including J. Mater. Chem. A, Appl. Surf. Sci, Mater. Horiz. and Nature Catal., mainly focusing on the prediction and catalytic properties of nanomaterials.

Dr Jian Zhou is a professor at the School of Materials Science and Engineering, Beihang University, China. He obtained his Ph.D. from the Institute of Metal Research, Chinese Academy of Sciences in 2003. He worked at RWTH Aachen University (Germany), Royal Institute of Technology (Sweden), and Xiamen University (China), before joining Beihang University. His research interests are two-dimensional transition metal carbides and borides (MXenes and MBenes), thermoelectric materials and intermetallics. Prof. Zhou has published over 160 peer-reviewed SCI papers, including four papers focusing on the prediction and applications for energy storage and catalysis of MBenes.

a series of ternary transition metal carbides and nitrides, with the atomic structures of alternate stacks of $M_{n+1}X_n$ and A layers, where A represents an element from the main groups (aluminum mostly) or Zn.[12] By removing the A atomic layers from MAX phases and separating the remaining $M_{n+1}X_n$ layers from each other, pristine MXenes could be obtained, with the atomic structures of alternate stacks of $n + 1$ layers of M and n layers of X, inherited from the MAX phases. Since the removal of A atomic layers is usually achieved by selective etching in aqueous solutions, the highly reactive transition metal surfaces are prone to be terminated by the groups in the etchants, resulting in the formation of surface terminations such as O, OH, F, *etc.*[11,13] The multiple compositions and structures endow MXenes with fascinating properties and thus they have been applied in diverse fields, such as energy,[14–16] electronics,[17,18] catalysis,[19–22] environment,[23,24] *etc.*

Inspired by the success of MXenes, people have been trying to expand X further to other elements. In 2017,[8] we reported a new kind of 2D transition metal boride analogue of MXenes for the first time, and coined a catchy name, MBenes, to emphasize their 2D morphology. By means of first principles calculations, it was found that four kinds of MBenes, Cr_2B_2, Fe_2B_2, Mo_2B_2 and W_2B_2, were expected to be obtained from Cr_2AlB_2, Fe_2AlB_2, MoAlB and WAlB by selective etching methods, which was later applied for the successful synthesis of 2D Cr_2B_2 and Mo_2B_2 by Zhang *et al.*[9] and Alameda *et al.*[10] The three pioneering studies opened the gate of research on MBenes. Thereafter, more and more new orthorhombic and hexagonal MBenes were found successively. To date, MBenes have become a big family with over 50 members, with the general formula of M_nB_{2n-2}, where M represents transition metal, B represents boron and $n = 2, 3, 4$.

Over the past five years, MBenes have attracted more and more attentions of both theoretical and experimental researchers in the fields of nanomaterials, physics and chemistry. The structural, mechanical, electronic and magnetic properties, and applications for energy storage and electrocatalysis of MBenes have been widely explored. However, we have noticed that MBenes are usually confused with other 2D transition metal borides,[25–28] which originates from the lack of a clear definition of MBenes. Besides, there lacks specific review work on MBenes. Therefore, here we present a review on the progress, challenges and future of MBenes.

In this review, first we proposed an explicit definition of MBenes and classified them into two categories, orth-MBenes and hex-MBenes, by briefly reviewing the discovery history of the MBenes family. Then the experimental synthesis methods, structural, mechanical, electronic and magnetic properties of MBenes were summarized and discussed. After that, we gave an overview of applications for energy storage and electrocatalysis of MBenes. Finally, discussions and perspectives on the existing problems, major challenges and future development of MBenes were provided.

2 What are MBenes?

The first-reported MBenes contain orthorhombic Cr_2B_2, Mo_2B_2, W_2B_2 and Fe_2B_2. They have common features such as orthorhombic crystal systems, sandwich-like layered structures, M_2B_2-type chemical formula and MAB phases as precursors.[8] Then M_3B_4-type, M_4B_6-type orthorhombic MBenes and hexagonal MBenes have been reported in succession. However, there has not been an explicit definition of MBenes until now. On the other hand, MBenes have been misused to describe other 2D transition metal borides in some studies. Therefore, here we present a scientific classification and an explicit definition of MBenes by briefly reviewing the development history of MBenes. Based on the definition, other 2D transition metal borides could be distinguished from MBenes.

Since MXenes are derived from MAX phases, to obtain 2D transition metal borides, layered ternary transition metal borides are indispensable. Fortunately, there exist a series of layered 3D ternary transition metal borides with orthorhombic structures. In 2015, Hillebrecht *et al.*[29] investigated Cr_2AlB_2, Cr_3AlB_4, Cr_4AlB_6, MoAlB, WAlB, Mn_2AlB_2 and Fe_2AlB_2, which are composed of alternate stacks of M_2B_2 layers and Al layers. Due to the high structural similarity to MAX phases, these ternary transition metal borides were named as "MAB phases". As shown in Fig. 1(a), there are six types of orthorhombic MAB phases: M_2AB_2, $M_2A_2B_2$, $M_3A_2B_2$, M_4AB_4, M_3AB_4 and M_4AB_6, in which transition metal boride layers and A or A_2M layers stack alternately. To date, most of the MXenes have been synthesized from MAX phases by etching methods, which is attributed to the nature of different bond strengths between M–X and M–A bonds. In MAX phases, M–X bonds show mixed characteristics of covalent and ionic bonds while M–A bonds are metallic. Therefore, M–X bonds are stronger than M–A bonds, making it

Dr Zhimei Sun is the Cheung Kong Scholar Chair Professor of the School of Materials Science and Engineering at Beihang University, China. Prof. Sun received her Ph.D. in Materials Science from the Institute of Metal Research, Chinese Academy of Sciences in 2002. Before joining Beihang University, she worked at RWTH Aachen University (Germany) and Uppsala University (Sweden) from 2002 to 2007, and Xiamen University (China) from 2007 to 2013. Prof. Sun's research interests include energy storage and catalysis of two-dimensional materials such as MBenes and MXenes, low-dimensional magnetic materials and phase-change materials for random access memory by both experiments and computational simulations. Prof. Sun is the pioneering and professional researcher in the MBene field, with 4 published research articles focusing on MBenes, including the first report of MBenes. Prof. Sun has published over 200 SCI papers including 4 papers in Phys. Rev. Lett., 4 papers in J. Am. Chem. Soc., and 47 papers in RSC journals.

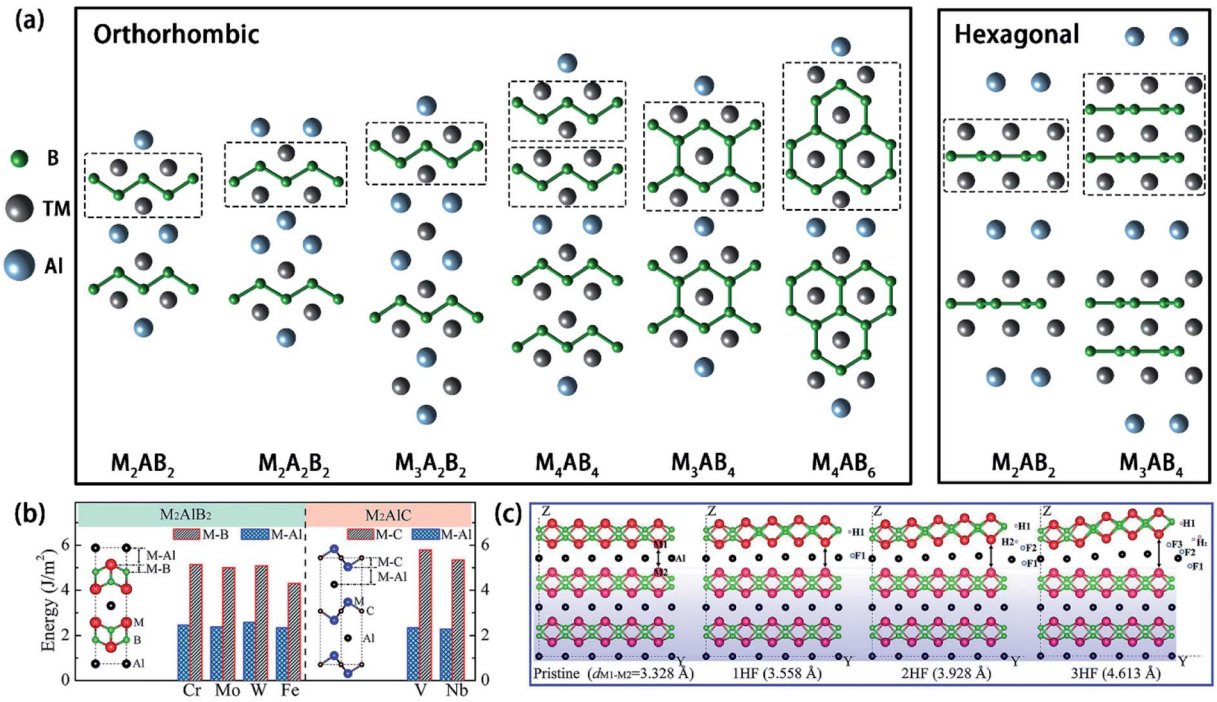

Fig. 1 (a) Structures of orthorhombic and hexagonal MAB phases. (b) Bonding energy of M_2AlB_2-type orthorhombic MAB and M_2AlC-type MAX phases. (c) Simulated exfoliation process of orthorhombic M_2AlB_2 using HF, where the red, green, black, cyan, and pink balls represent Mo, B, Al, F, and H atoms, respectively. Reprinted with permission from ref. 8. Copyright (2017), Royal Society of Chemistry.

feasible to selectively etch out the A layers in MAX phases by breaking the M–A bonds while the M–X bonds remain intact. Due to the high similarity of composition and structures between MAX and MAB, it was found that the M–B bonds in the MAB phase are covalent bonds and ionic bonds with high binding strength while M–A bonds are metallic bonds with relatively weak binding strength, which is exactly the same as the situation in MAX phases. The similar bond nature of MAB offers the opportunity for synthesis of a new kind of 2D transition metal boride. Therefore, by separating the transition metal boride layers and A or A_2M layers, 2D transition metal borides are expected to be obtained.

From this point, we took the lead to explore the 2D transition metal borides derived from MAB phases. First, we investigated the bond energy of M–B and M–Al bonds in "M_2AlB_2" type MAB (M = Cr, Mo, W, Fe) and compared them with that of M–C and M–Al bonds in V_2AlC and Nb_2AlC.[8] As shown in Fig. 1(b), the results suggested that in MAB phases the bonding energy of M–B bonds is about twice as large as that of M–Al bonds, which is similar to the case of MAX phases. Therefore, we proposed that by a selective etching method, the Al atomic layers were expected to be removed from MAB phases and a new kind of 2D transition metal boride could be obtained. The simulation of HF intercalation *via* the M_2AlB_2 edge was also performed, as illustrated in Fig. 1(c). The derived 2D Cr_2B_2, Mo_2B_2, W_2B_2 and Fe_2B_2 inherit the orthorhombic structures from their parent MAB phases and were named as "MBenes".[8] The predication proposed by us was soon verified experimentally: 2D Cr_2B_2 and Mo_2B_2 MBenes were synthesized by room-temperature etching Cr_2AlB_2 and MoAlB with HCl and NaOH solution by Zhang *et al.*[9] and Alameda *et al.*,[10] respectively. In the MXene family, besides M_2X, there also exist M_3X_2, M_4X_3 and even thicker M_5X_4 MXenes. Therefore, our group further explored MBenes with more transition metal layers and two thick Cr-based MBenes, Cr_3B_4 and Cr_4B_6, derived from Cr_3AlB_4 and Cr_4AlB_6, respectively, further enriching the members of MBenes. To date, 24 MBenes with orthorhombic structures have been reported, including eighteen M_2B_2 (M = Sc, Ti, V, Cr, Mn, Fe, Co, Ni, Y, Zr, Nb, Mo, Tc, Ru, Rh, Hf, Ta, W),[8,30–35] five M_3B_4 (M = V, Cr, Mn, Nb, Ta)[33,36–39] and one M_4B_6 (M = Cr).[36] Although $CrMnB_2$ and $CrFeB_2$ were investigated, their stability has not been proved.[31] Therefore, here we exclude them from MBenes. Among the reported orthorhombic MBenes so far, 2D Cr_2B_2, Mo_2B_2 and Ti_2B_2 have been obtained experimentally.

On the other hand, exploration of hexagonal boride analogues of MXenes was first achieved by Bo *et al.*,[40] who have reported a series of hexagonal 2D M_2B_2, including Sc_2B_2, Ti_2B_2, V_2B_2, Cr_2B_2, Y_2B_2, Zr_2B_2 and Mo_2B_2, which are more similar to M_2X MXenes in structures. However, there lack the corresponding hexagonal MAB phases at that time. In 2019, Wang *et al.*[41] synthesized hexagonal Ti_2InB_2, which is the first and only synthesized hexagonal MAB phase so far. Although M_3AB_4-type hexagonal MAB phases were predicted to be stable, they were not synthesized yet. As shown in Fig. 1(a), similar to the orthorhombic MAB phases, it is also found that transition metal boride layers and A layers stack alternately in hexagonal MAB phases. Although it seems that Ti_2InB_2 could produce hexagonal 2D Ti_2B_2, in the experiment performed by Wang *et al.*,[41]

orthorhombic 2D Ti_2B_2, rather than hexagonal 2D Ti_2B_2, appeared after removal of the In layer through dealloying of Ti_2InB_2 at high temperature under a high vacuum. Nevertheless, hexagonal 2D Ti_2B_2 is verified to be stable theoretically by phonon dispersion and first-principles molecular dynamics (FPMD) calculations, which suggested that hexagonal 2D Ti_2B_2 might be a metastable phase while orthorhombic 2D Ti_2B_2 is thermodynamically more stable. Besides 2D hexagonal Ti_2B_2, there are another eleven 2D hexagonal M_2B_2 (M = Sc, Ti, V, Cr, Y, Zr, Nb, Mo, Hf, Ta, W, Gd),[41–45] and two 2D hexagonal M_3B_4 (M = Zr, Hf),[42] which were predicted to be stable theoretically.

Although different in crystal structures, the orthorhombic and hexagonal 2D transition metal borides have many similarities: (1) both of them have the chemical formula of M_nB_{2n-2}; (2) both of them have the corresponding MAB phases as precursors; (3) both of them have sandwich-like structures with the M–B_2–M–… stacking sequence. Therefore, here we suggest to classify both the orthorhombic and hexagonal 2D transition metal borides in the MBene family.

Here we further propose an explicit definition of MBenes: MBenes are a family of orthorhombic and hexagonal 2D transition metal borides derived from MAB phases with the unified chemical formula of M_nB_{2n-2} and structures of alternate stacks of transition metal and B layers, where M is transition metal, B is boron and n = 2, 3, 4. To distinguish MBenes by different crystal symmetries, MBenes can be divided into two categories: orthorhombic MBenes (orth-MBenes) and hexagonal MBenes (hex-MBenes). The precursors of orth-MBenes and hex-MBenes correspond to orthorhombic MAB (orth-MAB) and hexagonal MAB (hex-MAB), respectively. All the reported MBenes and their structures are shown in Fig. 2. It is noteworthy that other names have ever been used to describe MBenes, such as "boride MXenes"[41,42] and "boridene".[46] However, "boride MXenes" neglect the obvious differences in both structures and chemical formulas between MXenes and MBenes while "boridene" contains all the 2D borides. Therefore, it is more appropriate to describe these new 2D transition metal borides with the name "MBenes", which not only indicates their compositions explicitly, but also demonstrates both similarity and difference to MXenes.

Besides the typical M_nB_{2n-2}-type MBenes, there also exist fourteen predicted $(M'_{2/3}M''_{1/3})_2B_2$, where M′ represents Ti, Cr, Mn, Fe, Mo, W and M″ represents Sc, Y, Zr, Nb, Hf,[47] and one synthesized $M_{4/3}B_2$, where M = Mo.[46] These fifteen 2D transition metal borides were derived from the corresponding quaternary hex-MAB phases, $(M'_{2/3}M''_{1/3})_2AlB_2$,[47,48] and have structures similar to hex-MBenes and in-plane ordered double metal elements or vacancies, as shown in Fig. 3. Among the 14 $(M'_{2/3}M''_{1/3})_2B_2$, $(Fe_{2/3}Sc_{1/3})_2B_2$ belongs to the $P6mmm$ (191) space group while the other 13 belong to the $P\bar{3}m1$ (164) space group. Based on the structural characteristics, they should also be classified into MBenes, denoted as in-plane ordered hex-MBenes.

It is noticed that there are many other 2D transition metal borides, which are sometimes mistaken as MBenes. We should be aware that MBenes do not represent all the 2D transition metal borides, which is similar to the situation that MXenes do not represent all the 2D transition metal carbides because 2D transition metal carbides such as 2D MC_2 (TiC_2[49] MoC_2 (ref. 50)) do not belong to MXenes. Based on the definition and characteristics of MBenes mentioned above, we can distinguish MBenes from other 2D transition metal borides. Firstly, 2D Ti_2B,[27] Mo_2B[51] and Hf_2B[42] should be classified as new boron-containing MXenes since they have exactly the same

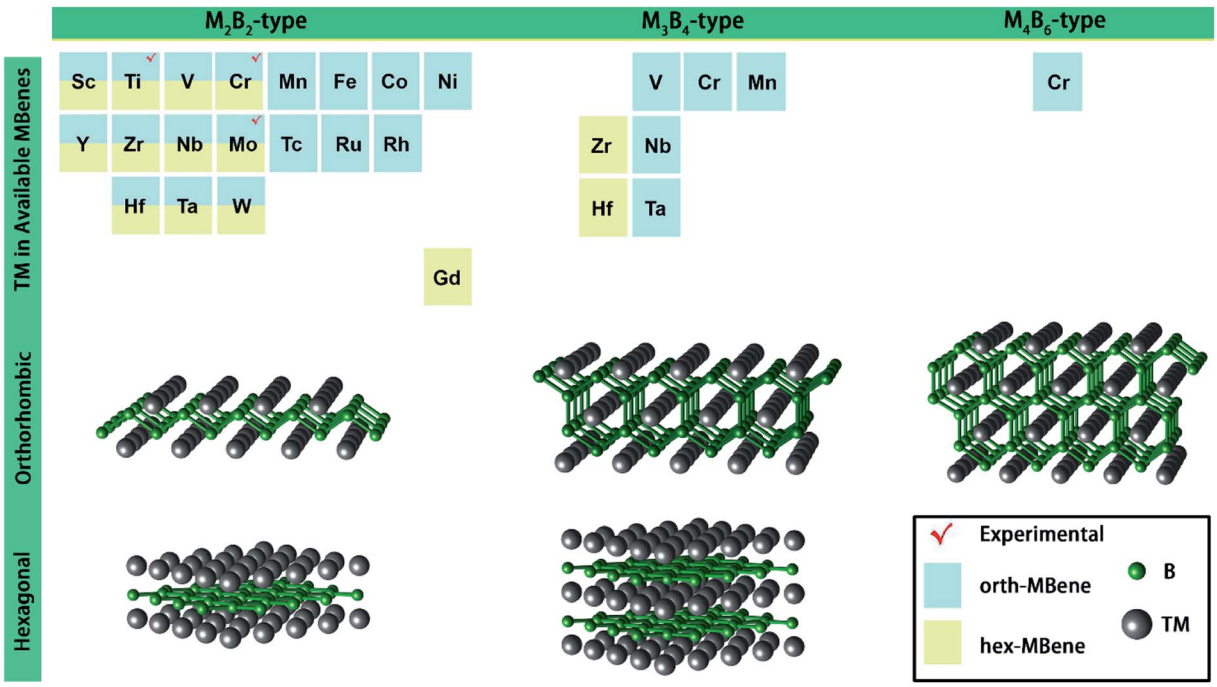

Fig. 2 Atomic structures of all the reported orth-MBenes and hex-MBenes so far.

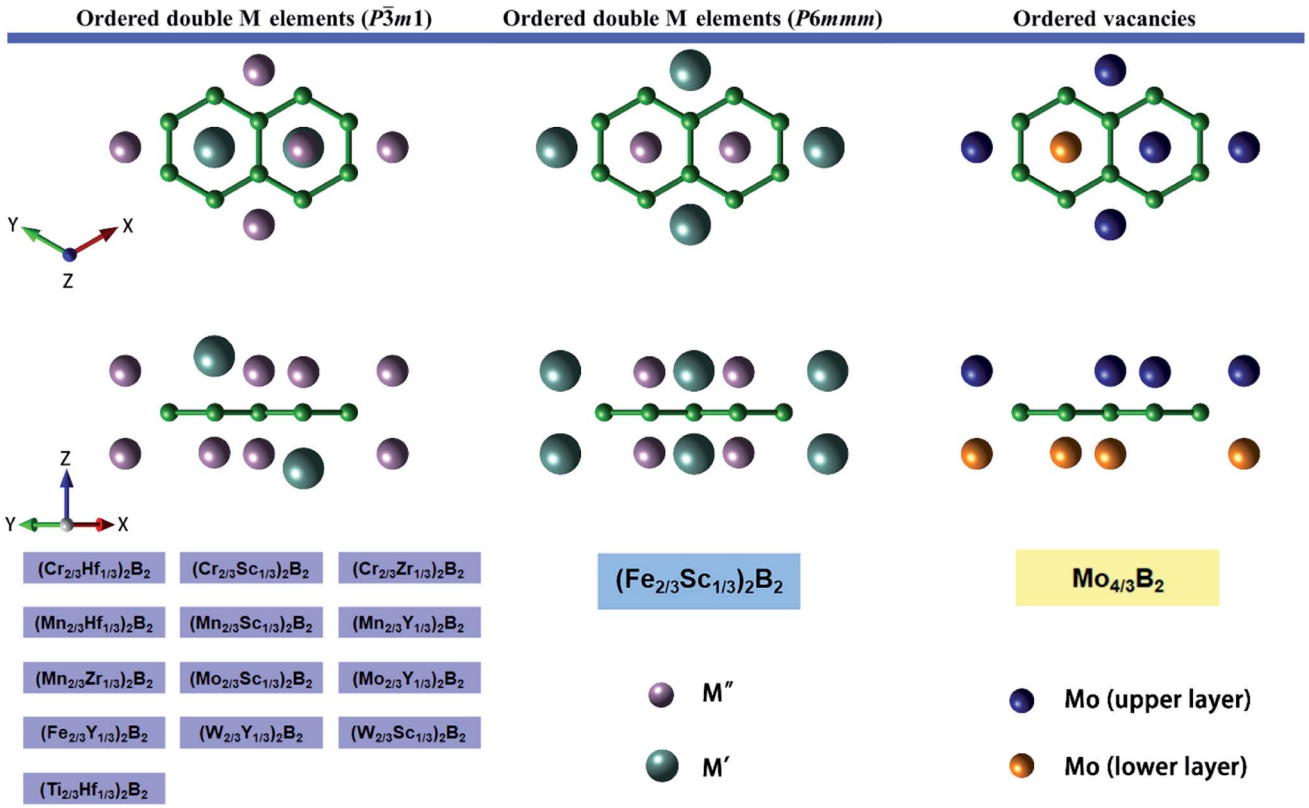

Fig. 3 Structures of hex-MBenes with in-plane ordered double metal elements and vacancies.

structures and chemical formula as typical M_2X MXene. Secondly, 2D LiB[52] and NiB[26] have no layered structures of alternate stacks of transition metal and B layers. Additionally, 2D MgB_2,[53] FeB_2,[54] TiB_2,[25] and tetragonal Mn_2B_2 (ref. 28) have no corresponding MAB precursors. Some other 2D transition metal borides including M_5B_2, $M_{10}B_4$, MB_6, *etc.*[31,33,37] have very different structures and compositions from those 2D transition metal borides derived from MAB phases. Therefore, they should also be excluded from the MBene family.

3 Synthesis of MBenes

Among 50 reported MBenes, Cr_2B_2, Mo_2B_2 and Ti_2B_2 orth-MBenes, and $Mo_{4/3}B_2$ hex-MBenes have been synthesized, while no M_3B_4/M_4B_6 orth-MBenes or M_2B_2/M_3B_4 hex-MBenes are available experimentally. However, it is interesting that these four MBenes were obtained from different kinds of MAB phases and by different synthesis methods.

Low-temperature etching

Among the four synthesized MBenes, orthorhombic Cr_2B_2, Mo_2B_2 and hexagonal $Mo_{4/3}B_2$ were synthesized by a low-temperature etching method. The etchants for Cr_2B_2 and Mo_2B_2 synthesis were HCl and NaOH solutions, respectively, while that for hexagonal $Mo_{4/3}B_2$ was HF solution, which has been widely used for the synthesis of MXenes. Moreover, they are obtained from different types of MAB phases: Cr_2AlB_2 (M_2AB_2-type orth-MAB), MoAlB ($M_2A_2B_2$-type orth-MAB) and $(Mo_{2/3}Y_{1/3})_2AlB_2$ (quaternary hex-MAB phases) respectively.

In Cr_2AlB_2, Al and Cr_2B_2 layers stack alternately, which is similar to the alternate stack of Al and M_2X layers in 211-type MAX phases. Therefore, the synthesis process for Cr_2B_2 is very similar to that for MXenes. Zhang *et al.*[9] synthesized Cr_2AlB_2 from CrB and Al powders first. Then hydrochloric acid was selected as an etchant because of its safety and environmental benignity. By immersing the Cr_2AlB_2 powder in dilute HCl solution (1.25 mol L^{-1}) for 6 h at room temperature, followed by post-processing of centrifuging the resulting suspension to separate the powder from the supernatant, and subsequent washing using de-ionized water several times before drying, a new phase that belongs to neither the Cr_2AlB_2 phase nor the CrB impurity phase was detected in the X-ray diffraction pattern. The EDS composition analysis indicated that the etched samples contained only 0.52% aluminum in weight, implying that the Al atomic layers were removed from Cr_2AlB_2. Fig. 4(a) and (b) show the scanning electron microscopy (SEM) images of the microstructures of Cr_2AlB_2 powder before and after HCl etching for 6 hours. Furthermore, it was found that by extending the immersing time in dilute HCl solution to 8 hours, most of the Cr_2AlB_2 converted to 2D Cr_2B_2, as shown in the X-ray diffraction pattern in Fig. 4(c). In addition, after stirring and/or ultrasonic treatment, much thinner 2D Cr_2B_2 with rolled-up shapes could be obtained, the SEM image of which is shown in Fig. 4(d).

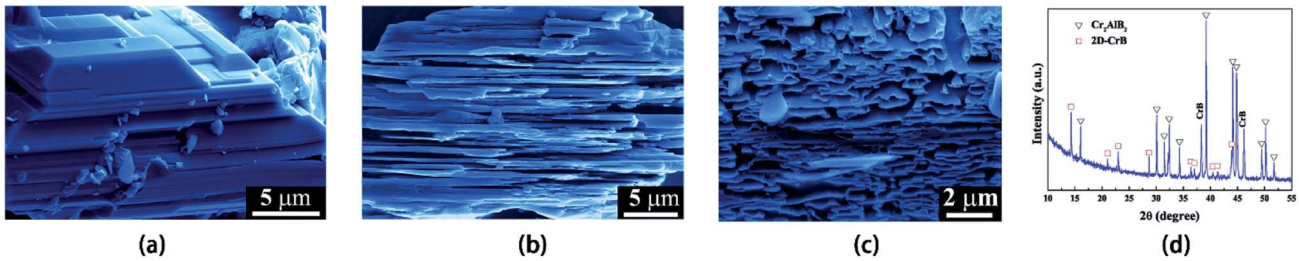

Fig. 4 SEM images of the microstructures of Cr_2AlB_2 powder (a) before etching and after treatment in diluted HCl (1.25 mol L^{-1}) solution for (b) 6 hours and (c) 8 hours. (d) X-ray diffraction pattern of samples after etching for 8 h in dilute HCl (1.25 mol L^{-1}) solution. Reprinted with permission from ref. 9. Copyright (2018) Elsevier.

The synthesis method for Cr_2B_2 is typical room-temperature etching used for most MXenes. However, there is a little difference for the situation of Mo_2B_2, which is due to the fact that in MoAlB, the Mo_2B_2 layers are separated by double layers of Al atoms. Intuitively, it would be more difficult to etch out the Al atoms in MoAlB than Cr_2AlB_2. Nevertheless, Mo_2B_2 nanosheets were still obtained through a room-temperature etching method.[10] In the etching process, stepwise deintercalation of Al was observed, and the reaction scheme is shown in Fig. 5(a). Before etching, stacking faults are sparsely distributed throughout the surface region of the MoAlB crystal. After 2 h with 10% NaOH of etching, the stacking faults increased and the "stacking fault bands" formed, which grew with etching time increasing until a high density of stacking faults were reached. Several metastable Mo–Al–B intergrowth phases including Mo_2AlB_2, $Mo_3Al_2B_3$, $Mo_4Al_3B_4$ and $Mo_6Al_5B_6$ appeared during the process and Mo_2AlB_2 was identified as the direct precursor for the synthesis of Mo_2B_2 orth-MBene. Then aluminum was removed from the stacking faults to form etched cavities. After treatment for 24 h, at the inner wall of etched cavities, split Mo_2B_2 monolayers were observed in the annular dark-field scanning transmission electron microscopy (ADF-STEM) image (Fig. 5(b)), indicating that synthesis and exfoliation of Mo_2B_2 orth-MBenes from MoAlB are indeed feasible. In the experiment, an aqueous solution of 10% NaOH and a solution of 2 M LiF in 6 M HCl were both used as etchants at room

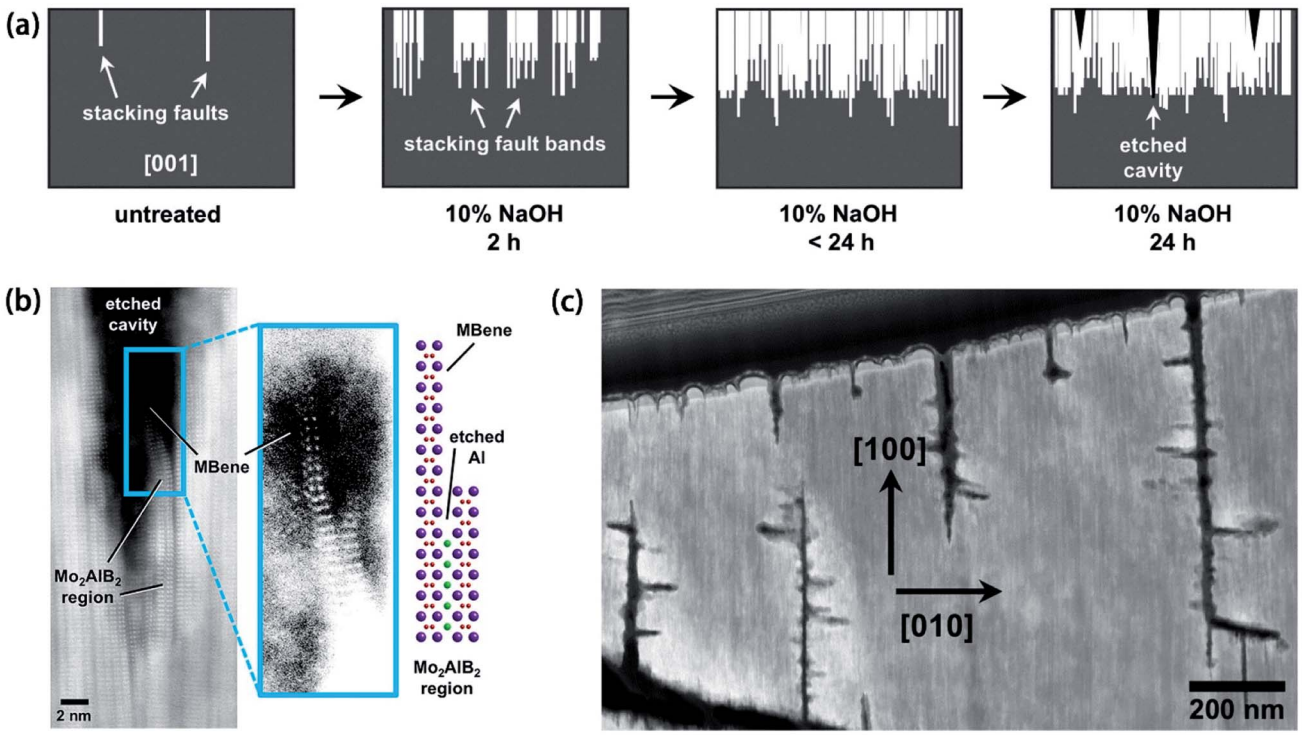

Fig. 5 (a) Reaction scheme of the process of topochemical deintercalation of Al from MoAlB treated with 10% NaOH solution. (b) ADF-STEM image of two isolated, delaminated Mo_2B_2 MBene sheets inside an etched cavity (left); higher-magnification and contrast-enhanced image of the cavity containing the MBene sheets (middle); idealized structure of the delaminated region of the MBene sheets (right). (c) ADF-STEM image of MoAlB after etching with a solution of LiF in HCl for 24 h. Reprinted with permission from ref. 10. Copyright (2018), American Chemical Society.

temperature. The post-processing includes vacuum filtration and rinse with deionized water, the same as the post-processing for Cr_2B_2. However, the LiF/HCl etchant led to so strong reaction that the molybdenum boride layers were even corroded. It was observed that etched "branches" propagated in the [010] direction of MoAlB, corroding through MoB layers to form a network of cavities, as shown in Fig. 5(c). When using 10% NaOH solution, no corrosion of MoB layers was observed. Therefore, compared to LiF/HCl, NaOH solution is more suitable for deintercalation of Al from MoAlB.

The synthesis of $Mo_{4/3}B_2$ was achieved by etching $(Mo_{2/3}Y_{1/3})_2AlB_2$ with 40 wt% HF solutions in an oil bath at 33 to 35 °C. Similar to the synthesis of $M_{1.33}C$ MXenes from i-MAX phases,[55] the Y and Al atoms were etched out together from $(Mo_{2/3}Y_{1/3})_2AlB_2$. After delamination, the obtained products were corroborated to be freestanding 2D molybdenum boride sheets larger than 50 nm, with some boron vacancies and mixed terminations of –O, –OH and –F. Therefore, the formula of the 2D molybdenum boride is referred to as $Mo_{4/3}B_{2-x}T_z$. The structure of $Mo_{4/3}B_2$ without boron vacancies and surface terminations is shown in Fig. 3.

High-temperature dealloying

To synthesize 2D Ti_2B_2, Wang *et al.*[41] first examined the stability of a series of 3D $Ti_xA_yB_z$ phases and Ti_2InB_2 was identified as the only thermodynamically and dynamically phase at ambient pressure. Then Ti_2InB_2 was synthesized through a solid-state reaction from a mixture of Ti, In and B powder. Interestingly, the hexagonal structure (space group of $P\bar{6}m2$) was confirmed both theoretically and experimentally, exhibiting a different structure from M_2AB_2-type orth-MAB phases, which could be observed from the high-angle annular dark-field scanning transmission electron microscopy (ADF-STEM) image along the [001] direction and a fast Fourier transform (FFT) of the HAADF image in Fig. 6(a). Therefore, Ti_2InB_2 was expected to serve as the precursor of Ti_2B_2 hex-MBene. However, the conventional etching method did not work for Ti_2InB_2: after immersing Ti_2InB_2 powder in 50% HF at room temperature for 12 h, Ti_2InB_2 was totally dissolved and no new phase was generated. To obtain 2D Ti_2B_2, a dealloying strategy was applied considering indium has the nature of low melting point and high vapor pressure. As expected, at 1050 °C for 6 days under vacuum conditions about 10^{-4} Pa, indium atoms were almost completely removed from Ti_2InB_2. However, besides the impurity phases, the obtained products were TiB compounds with an orthorhombic structure, most of which belong to the *Cmcm* space group with a small amount belonging to the *Pnma* space group, rather than the hexagonal structure, as illustrated in Fig. 6(b). This indicated that the local displacement of Ti and B atoms occurred during the high-temperature dealloying process, leading to a phase change from hexagonal to orthorhombic. The SEM image of the 2D TiB phase is shown in Fig. 6(c), along with the atomic ratio, indicating that nearly no B deficiency formed and little In remained during the high-temperature dealloying process. Fig. 6(d) shows the high-resolution transmission electron microscopy (HRTEM) image along the $[01\bar{1}]$ direction and the inset shows the selected area electron diffraction (SAED) pattern of the selected area. Nevertheless, hexagonal Ti_2B_2 ($P\bar{6}m2$) was proved to be thermodynamically and dynamically stable by first principles calculations. The interlayer slip, collapse of boron hexagonal rings and formation of boron chains were found by first-principles molecular dynamics simulations, which implies that the *Cmcm* phases might originate from the $P\bar{6}m2$ phases.

4 Structures & properties

MBenes have typical sandwich-like structures like MXenes with the alternating stacking sequence of $M–B_2–M(–B_2–M)_n$ ($n = 0, 1, 2$). However, the stoichiometries of MBenes are different from those of MXenes, resulting in great structural discrepancies between them. On the other hand, there also exist obvious differences between the structures of orthorhombic and hexagonal MBenes, although they have the same stoichiometries and stacking sequences of atomic layers. Besides the difference in crystal systems, in orth-MBenes, transition metal layers are separated by double B atomic layers and the distance between the nearest B atoms in two layers (d_2) is much smaller than that in a single layer (d_1), while for hex-MBenes, the B atoms form flat single layers with honeycomb structures, as shown in Fig. 7(a). It is widely known that MXenes are prone to be terminated by surface functional groups such as O, OH and F during the etching process. With the exposed transition metal

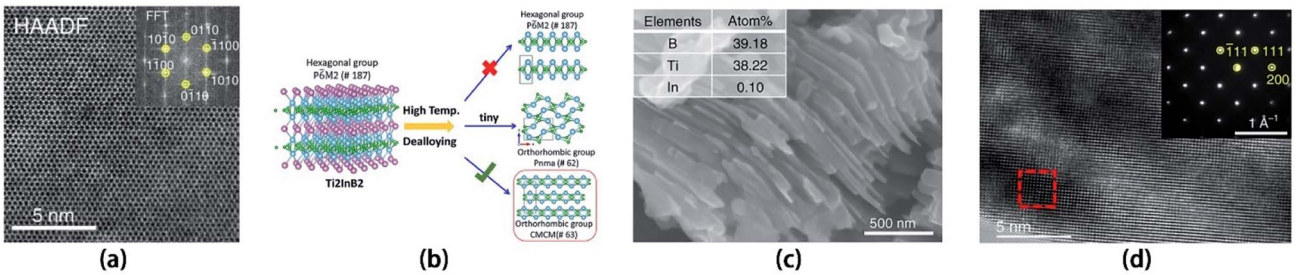

Fig. 6 (a) HAADF image of Ti_2InB_2 along the [001] direction and the inset shows the corresponding FFT pattern. (b) Schematic of the high temperature dealloying process of Ti_2InB_2. (c) SEM image of the Ti_2B_2 sheets with treatment at 1050 °C for 6 days under vacuum conditions about 10^{-4} Pa and the inset is the atomic ratio of the sample. (d) HRTEM image of the Ti_2B_2 sheets along the $[01\bar{1}]$ direction and the inset shows the SEAD pattern of the selected area. Reprinted with permission from ref. 41. Copyright (2019) Springer Nature.

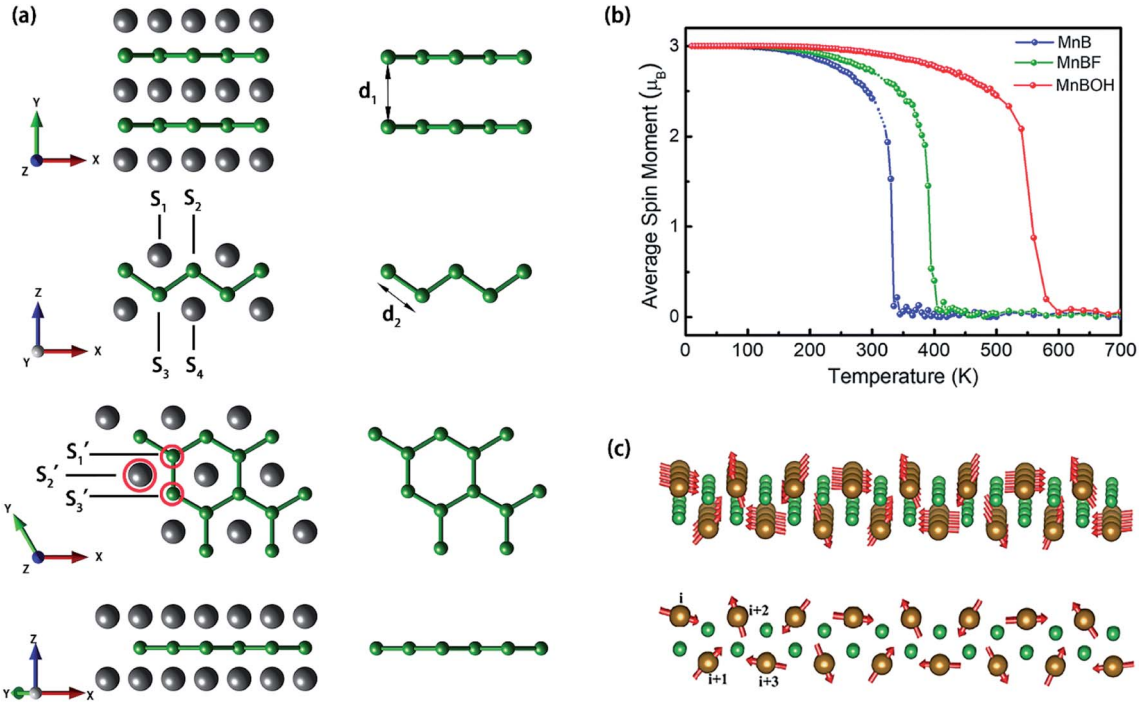

Fig. 7 (a) The structures of typical M_2B_2-type orth-MBenes and hex-MBenes along with the boron layers inside them and the sites of surface functional groups. (b) The relationship between average spin moment and temperature for Mn_2B_2, $Mn_2B_2F_2$ and $Mn_2B_2(OH)_2$ orth-MBenes. Reprinted with permission from ref. 38. Copyright (2018), Royal Society of Chemistry. (c) The perspective top view (top) and side view (down) of CAFM spin configurations for Fe_2B_2 orth-MBene, where Fe and B atoms are represented by the gold and green balls, respectively. *i* is the number of certain individual column. Reprinted with permission from ref. 57. Copyright (2021), American Physical Society.

layers, MBenes could also be terminated by functional groups. However, no surface functional groups have been tested in experiments for Cr_2B_2, Mo_2B_2 and Ti_2B_2 orth-MBenes.[9,10,41] Theoretically, there are four sites for functional groups on the surface of orth-MBenes, S1 site (on the top of M atoms of the upper layer), S2 site (on the top of B atoms of the upper layer), S3 site (on the top of B atoms of the lower layer) and S4 site (on the top of the M atoms of the lower layer), as displayed in Fig. 7(a). Considering the symmetry of orth-MBenes, the functional groups on both sides are located at the same site. The specific locations depend on the species of both functional groups and MBene substrates. For functionalized hex-MBenes, there are three different models with high symmetry. In models 1 and 2, terminations on both sides are located on the same site: top of M atoms (S_1') and the same B atom (S_2' or S_3'), respectively, while in model 3, one termination is located on S_2' while the other termination is located on S_3' in a unit cell. For most F/O/OH-functionalized hex-MBenes, models 2 and model 3 are more stable than model 1, except for $Mo_2B_2(OH)_2$, $W_2B_2F_2$ and $Mo_2B_2(OH)_2$, for which model 1 is the most favorable configuration. Like MXenes, the surface functional groups play key roles in manipulating the mechanical, electronic, magnetic properties and the performance for energy storage and electrocatalysis of MBenes.

The mechanical properties including Young's modulus, shear modulus, elastic constants and Poisson's ratio of both orthorhombic and hexagonal MBenes have been widely studied.[8,30,36,44] It was found that orth-MBenes are anisotropic while hex-MBenes are isotropic. The Young's modulus of pristine MBenes ranges from 150–350 N m^{-1} and increases with thickness.[8,36] Furthermore, Khaledialidusti *et al.*[44] investigated the mechanical properties of the hex-MBenes (M = Sc, Ti, Zr, Hf, V, Nb, Ta, Mo, and W) functionalized by F, O, and OH groups, and found that surface functional groups significantly influence the mechanical properties of hex-MBenes. Generally, compared with the pristine hex-MBenes, the O and OH functionalized hex-MBenes are mechanically stiffer and less ductile with a higher Young's modulus and shear modulus. The influences of surface functional groups on elastic constants and Poisson's depend on the composition and functional groups of MBenes.

All the pristine orthorhombic and hexagonal MBenes are metallic systems. However, after termination by certain surface functional groups, transitions from metallic to semimetallic or semiconductive occur for some MBenes, which is similar to the situation for MXenes. $Sc_2B_2O_2$, $Sc_2B_2F_2$, $Sc_2B_2(OH)_2$, $Zr_2B_2O_2$, and $Hf_2B_2O_2$ hex-MBene are found to be semimetal systems with the Perdew–Burke–Ernzerhof (PBE) functional by Khaledialidusti *et al.*,[44] who attribute the metal–semimetal transition to the effect induced by the F/OH/O groups, which can pop out the electrons from the occupied d band below the Fermi energy and/or from the π^* band states of boron atoms, making these bands become unoccupied and as a result, the functionalized MBenes show semimetal behavior. The Heyd–Scuseria–

Ernzerhof (HSE) screened hybrid functional was further used to study the band structure and it was found that $Sc_2B_2O_2$ becomes a semiconductor with an indirect bandgap of 0.5 eV while $Sc_2B_2F_2$, $Sc_2B_2(OH)_2$, $Zr_2B_2O_2$, and $Hf_2B_2O_2$ remain semimetallic.

There are many Cr/Mn/Fe-based systems in the MBene family, including Cr_2B_2, Cr_3B_4, Cr_4B_6, Mn_2B_2, Mn_3B_4 and Fe_2B_2 orth-MBenes, which show intriguing magnetic properties. Mn_2B_2 was found to be ferromagnetic[38,39] while Mn_3B_4 is antiferromagnetic.[39] Importantly, the pristine and OH/F-functionalized Mn_2B_2 possess Curie temperatures (T_C) above room temperature (345–600 K), as displayed in Fig. 7(b). Cr_2B_2, Cr_3B_4 and Cr_4B_6 were reported to be ferromagnetic systems by Zhang *et al.*[36] and the T_C values of Cr_2B_2, $Cr_2B_2(OH)_2$ and $Cr_2B_2F_2$ were further estimated to be 520 K, 570 K and 580 K, respectively by Dou *et al.*[56] However, Cr_2B_2 was reported to be antiferromagnetic by Liu *et al.*[39] Contradictory results of the magnetic ground state were also found for Fe_2B_2. According to the calculation results by Guo *et al.*,[8] Fe_2B_2 shows ferromagnetism, but it was reported to be antiferromagnetic by Dou *et al.*[56] In addition, Ozdemir *et al.*[57] predicted an unusual columnar antiferromagnetic (CAFM) ground state for Fe_2B_2 with the critical temperature of 115 K, below which the spins of Fe atoms keep the same direction in each column but rotate in every other column by the same amount, as shown in Fig. 7(c). Besides, Gd_2B_2 hex-MBene was also predicted to be ferromagnetic with $T_C = 550$ K,[43] which is the only magnetic hex-MBene so far.

5 Applications for energy storage and electrocatalysis

The metallicity endows MBenes with intrinsic outstanding electrical conductivity. In addition, the fully exposed surface is excellent for adsorption of molecules and ions. Furthermore, the nature of large surface specific areas is in favor of atom or molecule adsorption. Therefore, MBenes are expected to be applied as electrode and electrocatalysis materials. The applications for energy storage and electrocatalysis have been widely investigated theoretically by first principles methods, including anodes of Li, Na, Mg ion batteries and Li–S batteries, as well as electrocatalysis for the hydrogen evolution reaction (HER),[8,30,36,39,58,59] oxygen evolution reaction (OER),[59] oxygen reduction reaction (ORR),[59] nitrogen reduction reaction (NRR),[31–33,35,54,60–63] carbon dioxide reduction reaction (CO_2RR),[64,65] nitric oxide reduction reaction (NORR),[34,66] and urea production.[67]

Energy storage

Exploring high performance electrode materials is of great importance for next generation renewable energy technologies. Rechargeable lithium-ion batteries (LIBs) have developed for over 30 years,[68] and the exploration for electrodes with higher performance keeps going on. One of the most important indicators for LIBs is the storage capacity of lithium. Due to the 2D nature, MBenes are expected to exhibit high theoretical gravimetric capacity for Li atoms. The theoretical gravimetric capacity of M_2B_2-type MBenes ranges from 265 mA h g^{-1} to 969 mA h g^{-1}. It was reported that both orthorhombic and hexagonal Ti_2B_2 MBenes can accommodate only one layer of Li atoms[40,41] while Cr_2B_2, Mn_2B_2, Fe_2B_2, Mo_2B_2 orth-MBenes and Hf_2B_2 hex-MBene could accommodate up to two layers of Li atoms.[8,42,69] Surprisingly, V_2B_2 orth-MBene and Y_2B_2, Zr_2B_2 hex-MBenes could accommodate up to three layers of Li atoms at most without any structural distortion and the theoretical gravimetric capacities of them reach as high as 969, 806 and 654 mA h g^{-1}, respectively,[42,45,69] which are much higher than those of the commercial anode material, graphite (372 mA h g^{-1}) and the conventional Ti_3C_2 MXene (320 mA h g^{-1}).[70]

Another key indicator for evaluating the performance of an electrode material for LIBs is the charge–discharge rate, which relies on the diffusion barrier of Li atoms on the surfaces. It was reported that the diffusion barriers of Li atoms for hex-MBenes (17, 13 and 18 meV for hex-Ti_2B_2,[40] Y_2B_2[45] and Zr_2B_2,[42] respectively) are much lower than those for most orth-MBenes (210–290 meV),[8,69] Ti_3C_2 MXene (70 meV) and commercial graphite (about 300 meV).[70] In addition, the average open-circuit voltage (OCV) of hex-Y_2B_2 was calculated to range from 0.43–0.24 V, lower than the average value for Ti_3C_2 MXene (0.62 V) and comparable with that for graphite (about 0.2 V). In particular, Y_2B_2 hex-MBenes show not only high capacity, but also a low diffusion barrier and OCV, as shown in Fig. 8(a)–(c).

Although LIBs have the advantages of high energy density, long lifespan, and wide voltage window, they face the problems of safety and scarcity of lithium. Therefore, Na, K, Mg, Ca and Al ion batteries were explored as alternatives to LIBs due to the rich reserves of these metals.[13] The performances of pristine MBenes as electrodes of Na/Mg ion batteries were evaluated, and their theoretical gravimetric capacity are generally lower than that of LIBs because of the high atomic mass of Na/Mg than Li. For the Na ion battery (NIB), V_2B_2 orth-MBene has the maximum theoretical gravimetric capacity of 614 mA h g^{-1} with up to three layers of Na atoms adsorbed on the surface stably.[69] Similar to the situation for LIBs, the diffusion energy barrier for Na atoms on hex-MBenes is much lower than that on orth-MBenes,[41,45,69,71] and compared with LIBs, the diffusion energy barriers for Na atoms and OCV of NIBs are relatively lower than those of LIBs.[41,69,72] In addition, the performances for the Mg ion battery of Cr_2B_2/Mo_2B_2 orth-MBenes were investigated by Li *et al.*[72] The theoretical gravimetric capacity, diffusion energy barrier of Mg atoms and average OCV of MIBs were reported to be 853.4/502.1 mA h g^{-1}, 0.38/0.81 eV and 0.53/0.67 V, respectively.

The effects of functionalization on the battery performance of MBenes were further studied. It is found that after functionalization with O atoms, Mo_2B_2 and V_2B_2 orth-Mbenes maintain the maximum Li/Na adsorption quantity. However, the diffusion energy barrier for $Mo_2B_2O_2$ decreases while that for $V_2B_2O_2$ increases compared with pristine Mo_2B_2 and V_2B_2, respectively.[8,69] Furthermore, the values of OCV could be tuned with different surface functional groups. $Mo_2B_2O_2$ orth-Mbene possess high OCVs ranging from 3.2 to 2.2 V for the Na ion

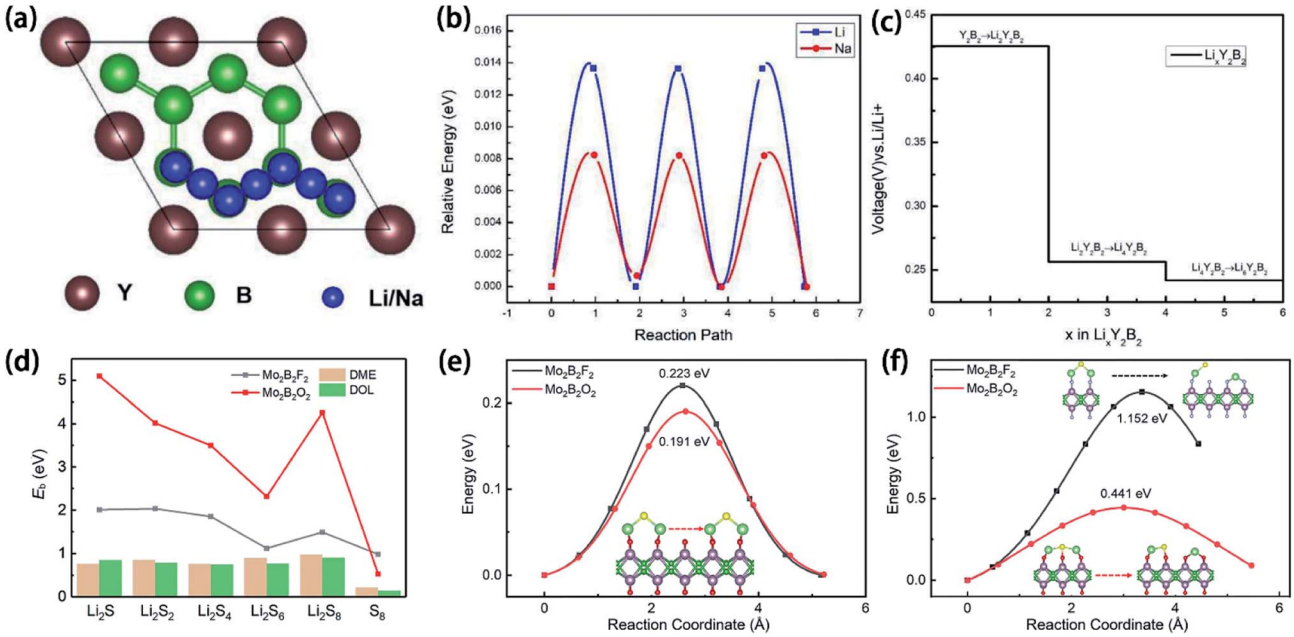

Fig. 8 (a) The diffusion path and (b) energy barrier curves of Li/Na on Y_2B_2 hex-MBene. (c) The OCV curves at different Li concentrations on Y_2B_2 hex-MBene. Reprinted with permission from ref. 45. Copyright (2021), Elsevier. (d) The binding energies (E_b) of S_8 and LiPSs on $Mo_2B_2O_2$ and $Mo_2B_2F_2$ MBenes compared with DME and DOL, two typical electrolyte molecules. (e) The diffusion energy curves along the [100] direction and (f) decomposition energy curves along the [010] direction of Li_2S on the surfaces of $Mo_2B_2F_2$ and $Mo_2B_2O_2$. The insets show the corresponding optimized structures. Reprinted with permission from ref. 74. Copyright (2021), Elsevier.

battery, meeting the requirement for cathode materials, while much lower OCVs of $Mo_2B_2S_2$, $Mo_2B_2Se_2$ and $Mo_2B_2Te_2$ (0.38, 0.23, and 0.08 V, respectively) for NIBs are suitable for anode materials.[73] Therefore, by modulating the surface functional groups, the desired performance for ion batteries of MBenes could be acquired.

In recent years, lithium–sulfur (Li–S) batteries have attracted more and more interest of researchers due to their ultrahigh theoretical capacity, which could reach several times of the commercial LIB. But their disadvantages lie in the poor electrical conductivity of sulfur, inevitable shuttling effect and inactive decomposition of low-order lithium polysulfide (LiPS). However, these obstacles could be effectively mitigated by functionalized Mo_2B_2 MBenes. Firstly, excellent metallic conductivity of functionalized Mo_2B_2 MBenes could be maintained before and after LiPS adsorption. Secondly, compared with typical electrolyte solvents (dimethyl ether and 1,3-dioxolane, *i.e.*, DME and DOL), $Mo_2B_2O_2$ and $Mo_2B_2F_2$ show more moderate binding strength as shown in Fig. 8(d), indicating that the shuttle effect could be suppressed and modulated by the surface functional groups. Finally, an ultra-low diffusion barrier (0.191 eV) and decomposition barrier (0.441 eV) of Li_2S cluster are achieved by $Mo_2B_2O_2$ as shown in Fig. 8(e) and (f), contributing to the capability and coulombic efficiency of Li–S batteries.[74]

Catalysis

Owing to the broad specific surface area, diverse surface chemical composition and metallic conductivity, MBenes have exhibited outstanding electrocatalytic activity towards various reactions, which could be applied for clean energy and chemical raw material production (HER, OER, NRR, CO_2RR, urea production), fuel cells (ORR) and pollution treatment (NORR).

The HER has become one of the most studied electrocatalytic reactions in recent years due to the significance of hydrogen generation. The most efficient catalyst for the HER is platinum, which is scarce and expensive, and there is a dire need for non-precious alternatives. Guo *et al.*[8] first studied the catalytic activity of Mo_2B_2, Fe_2B_2 and $Mo_2B_2O_2$, $Fe_2B_2O_2$ orth-MBenes for the HER. It is found that the bare surface of Mo_2B_2 binds with H atoms too strongly to desorb hydrogen. The inertia of Mo_2B_2 for HER becomes even severer after functionalized with oxygen due to the stronger binding strength between the surface O and H atoms. In contrast, Fe_2B_2 could provide relatively moderate affinity with H atoms ($|\Delta G_H|$ ranging from 0.001 to 0.038 eV, Fig. 9(a)), contributing to much higher activity than Pt ($|\Delta G_H| =$ 0.09 eV). The oxygen functionalization of Fe_2B_2 also results in stronger binding with H atoms (more negative ΔG_H), making $Fe_2B_2O_2$ inert for the HER. However, according to the surface Pourbaix diagrams studied by Guo *et al.*,[31] Fe_2B_2 can resist the surface oxidation under strong acidic conditions with 0 V *vs.* the standard hydrogen electrode (SHE), ensuring the surface not functionalized and high HER catalytic activity. In addition, the catalytic activity for the HER of Cr_2B_2 and Cr_3B_4, Cr_4B_6 orth-MBenes has been studied by Zhang *et al.*[36] Interestingly, the catalytic activity of these three Cr–B MBenes increases with thickness. Although Cr_2B_2 does not exhibit satisfactory catalytic activity due to the strong Cr–H interaction, with the increase of CrB_2 layers, the Cr–H bonds become weaker under various

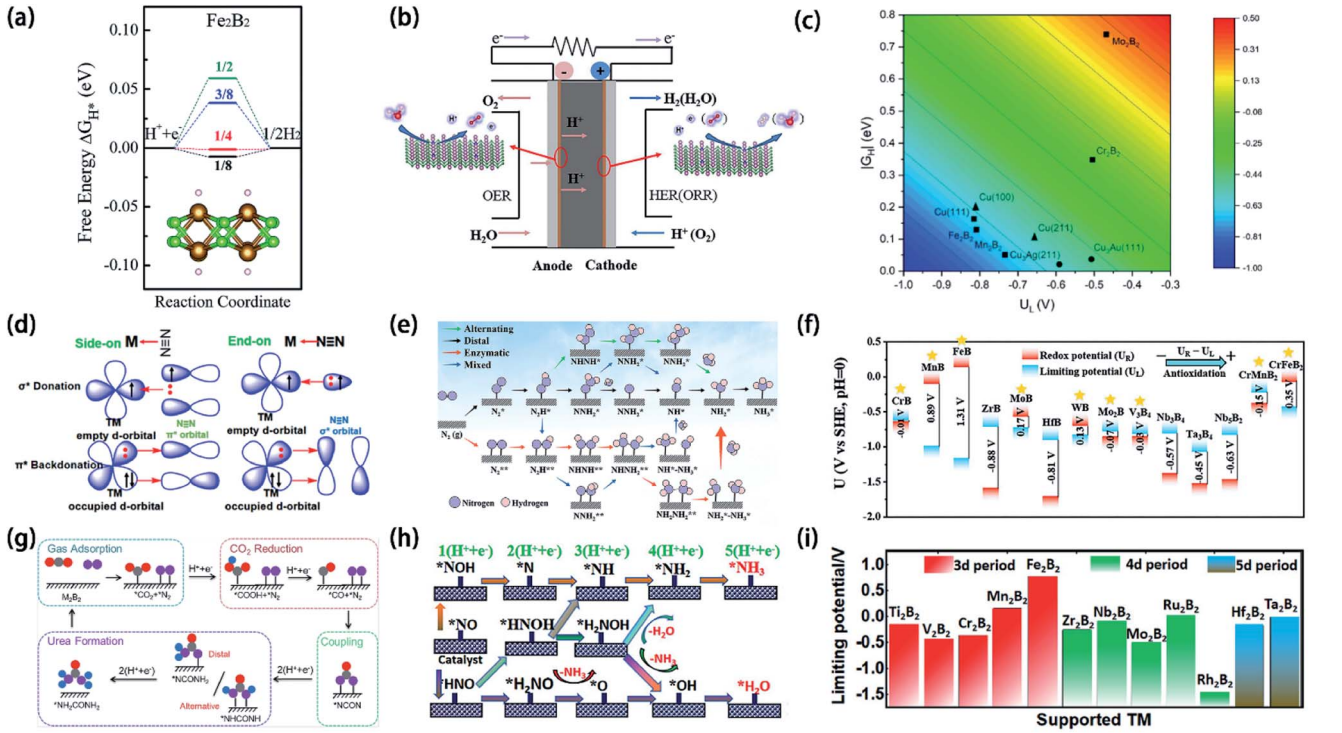

Fig. 9 (a) Gibbs free energy diagram for the HER of Fe_2B_2 orth-MBene at the equilibrium potential under different hydrogen coverages (1/8, 1/4, 3/8 and 1/2). The inset shows the atomic structures of Fe_2B_2 orth-MBene at 1/2 hydrogen coverage. Reprinted with permission from ref. 8. Copyright (2017), Royal Society of Chemistry. (b) Schematic for the application of HER/OER or OER/ORR bifunctional catalysts of TM@Mo_2B_2. Reprinted with permission from ref. 59. Copyright (2021), Royal Society of Chemistry. (c) Gradient graph combined with HER and CO_2RR performance for various orth-MBenes compared with some Cu-based catalysts. Reprinted with permission from ref. 64. Copyright (2021), American Chemical Society. (d) Schematic of the N_2 molecule activation mechanism for both side-on and end-on configurations on MBenes. Reprinted with permission from ref. 33. Copyright (2021), American Chemical Society. (e) Schematic of NRR. (f) Energy levels of theoretical limiting potential (U_L) and redox potential (U_R) of various orth-MBenes and other 2D transition metal borides. Reprinted with permission from ref. 31. Copyright (2021), Wiley. (g) Schematic of the mechanism of urea production from N_2 and CO_2. C, O, N, and H atoms are represented by the gray, red, pink, and blue balls, respectively. Reprinted with permission from ref. 67. Copyright (2021), Springer Nature. (h) Schematic of NORR. (i) Limiting potentials for NORR of M_2B_2-type MBenes *via* the most favorable mechanism. Reprinted with permission from ref. 34. Copyright (2021), Wiley.

hydrogen coverages. Surprisingly, the values of $|\Delta G_H|$ for Cr_4B_6 reach as low as 0.003–0.129 eV, showing promising potential to replace Pt for HER catalysis. For orth-Ti_2B_2, which has been obtained experimentally, Li *et al.*[30] confirmed that under zero potential, mixed O and OH terminations are more stable when pH < 3.6 while fully O terminations are more stable when pH > 3.6. Therefore, $Ti_2B_2O_2$ is the major state in realistic aqueous solutions. It is found that over a wide range of H coverages, $Ti_2B_2O_2$ exhibits extremely high catalytic activity with $|\Delta G_H|$ lower than 0.1 eV. Furthermore, the Tafel mechanism ($H^* + H^* \rightarrow H_2$) and Heyrovsky mechanism ($H^* + H^+ + e^- \rightarrow H_2$) of H_2 desorption were studied. The calculated results of activation barriers indicate that the Heyrovsky mechanism is more favored with a much lower activation barrier than the Tafel mechanism. Besides $Mo_2B_2O_2$, $W_2B_2O_2$ orth-MBene is also found to be inert for the HER due to too strong O–H bonds. To improve their catalytic activity, Li *et al.*[58] anchored single transition metal (TM) atoms on the surface of $Mo_2B_2O_2$ and $W_2B_2O_2$. By charge transfer from TM to O atoms, the O–H bonds get weakened, which favors the H adsorption. The improvements are more obvious on $W_2B_2O_2$ than $Mo_2B_2O_2$. While only Ti–$Mo_2B_2O_2$ shows HER catalytic activity, Ti/V/Zn/Cu/Ag/Au/Pt–$W_2B_2O_2$ all become active and some of them have multiple active sites.

The OER and ORR are the half-reactions for the water splitting process and fuel cells, respectively. However, Mo_2B_2 orth-MBene has too high overpotentials for the ORR and OER to be used as catalysts. Therefore, Zhang *et al.*[59] proposed a solution of embedding single 3d transition metal atoms at Mo vacancies to construct heterostructures, denoted as TM@Mo_2B_2, where TM represents 3d transition metals from Ti to Cu. Among 9 TM@Mo_2B_2, the overpotential for the OER of Ni@Mo_2B_2 and Cu@Mo_2B_2 is as low as 0.52 V and 0.31 V, respectively. For the ORR, Cu@Mo_2B_2 has an overpotential of 0.34 V. Compared with noble catalysts IrO_2 (η_{OER} = 0.56 V), RuO_2 (η_{OER} = 0.42 V) and Pt (η_{ORR} = 0.45 V), Ni@Mo_2B_2 has excellent OER catalytic activity and Cu@Mo_2B_2 is a promising bifunctional catalyst for both OER and ORR, which could be applied in fuel cells and metal–air batteries. Moreover, Ni@Mo_2B_2 also exhibits high HER catalytic activity, showing potential as a HER/OER bifunctional catalyst, desired for water splitting, as illustrated in Fig. 9(b).

Accompanied by the combustion of fossil fuels, CO_2 emission has become a problem that cannot be neglected. Electrochemical reduction of CO_2 to hydrocarbon fuels emerges as a strategy that could not only reduce the greenhouse effect, but also generate renewable energy resources. Reduction of one CO_2 molecule could lead to C1 hydrocarbon products including CO, HCOOH, HCOH, CH_3OH and CH_4. Liu *et al.*[64] investigated the catalytic properties for reducing CO_2 to CH_4 on Cr_2B_2, Mn_2B_2, Fe_2B_2 and Mo_2B_2 orth-MBenes, and Cu(111) was selected as the benchmark since it has the highest Faraday efficiency for methane. The results show that Cr_2B_2 and Mo_2B_2 possess not only higher catalytic activity for CO_2 reduction to CH_4, but also higher selectivity against the HER than Cu(111). Specifically, the limiting potential for Mo_2B_2 reaches −0.45 V, lower than those of a lot of Cu-based catalysts, as shown in Fig. 9(c). Xiao *et al.*[65] have investigated the CO_2RR catalytic properties along various pathways with different target products for two M_2B_2 (M = Zr, Hf) and three M_3B_4 (M = V, Nb, Ta) orth-MBenes. It is found that different materials show selectivity towards different products and V_3B_4 was considered as a promising candidate for CH_4 and CH_3OH production. In addition, suppressed HER could be achieved on all the investigated MBenes. Furthermore, ΔG_{*OH} and ΔG_{*CO} were assumed to be two key descriptors that determine the CO_2RR catalytic activity.

For a long time, the industrial production of ammonia has been dominated by the Haber–Bosch process ($N_2 + 3H_2 \rightarrow 2NH_3$), which requires high temperature and pressure, resulting in massive CO_2 emission and energy consumption. However, the NRR ($N_2 + 3H^+ + 3e^- \rightarrow 2NH_3$) could produce ammonia under room temperature and pressure, driven by electricity, and thus is expected to replace the conventional Haber–Bosch process. N_2 molecules could adsorb on the surface of catalysts with end-on or side-on configurations. According to the different N_2 adsorption configurations and sequences of interaction of proton/electron pairs and N atoms, there exist various reaction mechanisms, including distal, alternating and enzymatic mechanisms, *etc.* (Fig. 9(e)). From the equation $\Delta G = \Delta G^0 + k_B T \times \mathrm{pH} \times \ln 10 + eU$, to make the reaction spontaneous under pH = 0, the limiting potential $U_L = -\Delta G_{max}/e$ is required, where ΔG_{max} is the highest reaction Gibbs free energy during the whole NRR process, and lower U_L indicates higher catalytic activity. The NRR catalytic properties of MBenes have been studied by many researchers theoretically, which involves 20 M_2B_2 (M = Sc, Ti, V, Cr, Mn, Fe, Co, Ni, Y, Zr, Nb, Mo, Tc, Ru, Hf, Ta, W) and M_3B_4 (M = V, Nb, Ta) orth-MBenes as well as $Mo_2B_2O_2$-based SACs.[31–33,35,54,60–63] N_2 could be activated after adsorbing on the bare transition metal surfaces of MBenes by the "donation & back-donation" mechanism, in which N_2 molecules donate electrons from the σ* orbitals to the spare d orbitals in the transition metal atoms, while on the other hand, the occupied d orbitals of transition metal atoms back-donate electrons to the π* antibonding orbitals of N_2, as illustrated in Fig. 9(d). As a consequence, the N–N triple bonds in N_2 molecules are elongated and weakened, reducing the obstacles for the further hydrogenation process. It should be noted that the NRR is carried out in acid aqueous solutions, which gives rise to two issues: surface oxidation by O or OH groups and HER competition. For the first issue, Guo *et al.*[31] constructed surface Pourbaix diagrams and found that in the situation with 0 V *vs.* SHE, only Fe_2B_2 could resist surface oxidation. However, under the respective U_L for the NRR, Cr_2B_2, Mn_2B_2, Fe_2B_2, Mo_2B_2, W_2B_2 and V_3B_4 can all keep their surfaces from oxidation while Zr_2B_2, Hf_2B_2, Nb_3B_4 and Ta_3B_4 would be terminated by OH. The comparisons between U_L for NRR and U_R (redox potentials) are shown in Fig. 9(e), larger values of $U_R - U_L$ indicate stronger ability of antioxidation. For the HER competition issue, Guo *et al.* further suggest that more positive values of "$\Delta G_{H^*} - \Delta G_{N_2H^*}$" indicate higher selectivity towards the NRR and all the investigated MBenes except Mn_2B_2 and Fe_2B_2 were found to be highly NRR-selective. The affecting factors of U_L have been widely explored and many relationships have been established. Guo *et al.* correlate U_L with the d-band center of metal spin-α orbitals while Yang *et al.*[54] suggest that U_L values of MBenes are related to the work function, both the relationships are nearly linear. Qi *et al.*[32] have also reported the linear correlation between U_L and work function by the fitting expression $U_L = 0.27x + 0.1$ eV with an R^2 of 0.80, where x represents the work function of M_2B_2 (M = Sc, Ti, V, Y, Zr, Nb, Mo, Hf, Ta and W) orth-MBenes.

N_2 and CO_2 could not only be reduced to NH_3 and hydrocarbon products, respectively, but also to urea ($CO(NH_2)_2$) together, the mechanism schematic diagram of which is shown in Fig. 9(g). Zhu *et al.*[67] investigated the electrocatalytic properties for urea production on the three experimentally available orth-MBenes, Ti_2B_2, Cr_2B_2 and Mo_2B_2. The limiting potentials of −0.49 V for Mo_2B_2 and −0.52 V for Cr_2B_2 are even lower than that of the Pd–Cu catalyst (−0.64 V). Moreover, the competitive NRR, active site blockage by OH and self-corrosion under aqueous conditions can all be restrained on Cr_2B_2 and Mo_2B_2, indicative of their superior electrocatalytic activity, selectivity and stability towards urea formation.

Apart from N_2, nitric oxides could also be reduced to ammonia by electrocatalysis, referred to as the nitric oxide reduction reaction (NORR), which was reported to be more active than the NRR on Cu catalysts ($U_L = 0.9$ eV) by Long *et al.*[75] On the other hand, the NORR could also serve as an effective way to lighten air contamination caused by NO. He *et al.*[66] studied the NORR catalytic activity for Cr_2B_2, Mn_2B_2, Mo_2B_2, Hf_2B_2 and W_2B_2 orth-MBenes along two pathways, namely associative and dissociative pathways. When the NORR proceeds along the associative pathway, proton/electron pairs interact with N and O atoms of NO alternately, also resulting in two different sub-pathways involving the formation of HNO or NOH. In the dissociative pathway, the N–O bonds break after adsorption and three pairs of protons and electrons interact with the adsorbed N atom consecutively until the formation of NH_3. The maximum Gibbs free energy during the NORR on W_2B_2 was calculated to be only 0.37 eV along the dissociative pathway, and Mn_2B_2 exhibits even higher catalytic activity, with all the elementary reactions being exergonic along the associate pathway. Xiao *et al.*[34] studied the NORR catalytic properties of 12 M_2B_2 orth-MBenes where M represents Ti, V, Cr, Mn, Fe, Zr, Nb, Mo, Ru, Rh, Hf and Ta. However, they proposed enzymatic, distal, alternating, and hybrid pathways for the NORR, none of

which involve break of N–O bonds upon adsorption, as shown in Fig. 9(h). Among the investigated MBenes, Hf_2B_2, Nb_2B_2, Ta_2B_2 and Ti_2B_2 have extremely low limiting potential for the NORR towards NH_3 (U_L) and in particular, the NORR processes are totally spontaneous on Fe_2B_2, Mn_2B_2 and Ru_2B_2, exhibiting promising electrocatalytic activity for converting NO to NH_3, as shown in Fig. 9(i). In addition, the redox potentials of all the 12 MBenes are higher than their respective U_L, indicating the outstanding oxidation resistance of their surfaces. Also, most MBenes considered except Ti_2B_2, V_2B_2, and Zr_2B_2 show suppressed HER activity, ensuring their selectivity for the NORR.

6 Challenges & outlooks

The unique structural characteristics, intriguing properties and enormous potentiality for energy storage and electrocatalysis applications have made MBenes a new star in the world of 2D materials. Nevertheless, the exploration of these new 2D materials is still in the early stage. Challenges and opportunities coexist facing the unsolved issues and unexplored fields for MBenes. Herein, we discuss the existing problems of both experimental and theoretical research at the current stage. Perspectives are proposed to provide advice to address these issues. Furthermore, future research trends of MBenes, including new-type MBenes, synthesis, potential applications, phase change mechanisms and comparative study of hex-MBenes, orth-MBenes and MXenes with the same transition metal element are presented, aiming to inspire researchers in this field.

Above all, synthesis and characterization are the most fundamental part, and also the bottleneck for the development of MBenes. The first problem is the difficulty in etching MAB phases. It was found that 2 M LiF/6 M HCl solutions resulted in the corrosion of Mo_2B_2 layers, while orth-Mo_2B_2 has even not been fully etched out from MoAlB using 10% NaOH solutions,[10] which is not surprising since low concentration alkali could only etch the superficial layer of MAX phases.[11] But it has been proved that high alkali concentration and temperature to a certain extent would significantly improve the etching efficiency and yields for MXenes. For example, the yields of $Ti_3C_2T_x$ could reach 92% when etching Ti_3AlC_2 with 27.5 M NaOH at 270 °C.[76] Therefore, complete exfoliation of orth-Mo_2B_2 might be achieved by increasing the NaOH concentration and temperature. As for Ti_2B_2, it seems that phase change from hexagonal to orthorhombic occurs under high temperature.[41] Therefore, to synthesize hex-Ti_2B_2 from Ti_2InB_2, low-temperature etching methods under mild conditions should be applied. Since HF is known to be highly corrosive, use of HF solution with low concentration, shortening the etching time, reducing the temperature or replacing HF with a weakly corrosive etchant such as HCl or NaOH solutions are all expected to make the etching process less intensive.

Characterization of the synthesized samples is also critical. For orth-Mo_2B_2 and Ti_2B_2, no careful detection of the surface chemical position was performed experimentally. Although the theoretical work has showed that Cr_2B_2 is prone to be oxidized by OH without any applied voltage,[31] the EDS analysis results for Cr_2B_2 indicated that no OH or Cl was detected.[9] For the prepared samples, the characterization should also be paid attentions, especially for the identification of surface chemistry, which significantly affects various properties and performances for energy storage and electrocatalysis applications. In addition, vacancies and oxidization products, which are common in the etching process for MXenes, also deserve attentions for MBenes. First and last, comprehensive and systematic studies on MBenes synthesis and characterization are highly desired and should be given top priority.

For the theoretical research, there exist some contradictions and inadequacies in some studies that should be addressed. Orth-Cr_2B_2, Mn_2B_2 and Fe_2B_2 are the earliest reported MBenes, and their magnetic properties are critically important for electronics applications. However, the contradictions existing in different studies are very confusing. We summarized them in Table 1, from which we can see that all the contradictions originate from different calculation methods applied. It is widely known that the electronic and magnetic properties of systems containing transition metals are closely related to the localized (strongly correlated) electrons in d and f orbitals, which could not be well described with the GGA method. The most frequently used remedy is the DFT+U method, in which the value of U influences the total energy, electronic structures and magnetic ground states significantly. For the materials that have been obtained experimentally, the value of U is usually tested fitting the values of band gaps or magnetic moments by the DFT+U method with the experimental values. However, for some materials, there are not available experimental data. It should be noted that the value U varies with systems rather than elements, so it is not appropriate to apply the value of U in other systems, such as MXenes or oxides with the same TM to MBenes. As early as 2005, Cococcioni *et al.*[77] proposed a linear response approach to calculate the value of U, which could be achieved on various DFT software including ABINIT, Vienna *ab initio* simulation package (VASP), QUANTUM ESPRESSO, *etc.* It is suggested to calculate the value of U for strong-correlated systems, especially when studying the magnetic properties.

Although the electrocatalysis applications for MBenes have been widely studied theoretically, most of the research stays in fundamental stages and more realistic conditions should be taken into consideration. First of all, surface oxidation by OH or O groups in aqueous solutions is very common as previously mentioned and the surface chemistry would have great impact

Table 1 Summary of the magnetic ground states of Cr_2B_2, Mn_2B_2 and Fe_2B_2 orth-MBenes using different calculation methods

Systems	Magnetic ground state	Method	Reference
Cr_2B_2	Ferromagnetic	GGA+U ($U = 4$ eV)	36
	Ferromagnetic	GGA+U ($U = 3$ eV)	56
	Antiferromagnetic	GGA	39
Mn_2B_2	Ferromagnetic	GGA+U ($U = 2$ eV)	38
	Ferromagnetic	GGA	39
Fe_2B_2	Ferromagnetic	GGA	8
	Antiferromagnetic	GGA & HSE	57

on the electrocatalytic properties for various reactions. Since the characterization of surface chemistry is unavailable in experiments for MBenes so far, the surface Pourbaix diagrams combining the limiting potentials of various reactions could help to identify the practical composition of MBenes in the study of electrocatalytic properties. Secondly, vacancies of surface terminations and transition metal atoms are very common during the etching process, which could endow the materials with special properties. For example, vacancies could serve as active sites for molecule adsorption and modifying atoms; surface terminations around the vacancies always exhibit distinct charge states compared with other terminations. Anyway, vacancies should be paid special attentions since they are very common in practice. Surfaces do not exist in practical applications. In addition, for most reactions, the sluggish kinetics is the key factor that restricts the reaction rate, especially for water splitting. Therefore, besides Gibbs free energy, energy barriers should also be carefully evaluated, which could be achieved by NEB or CINEB methods. Furthermore, all the studies on catalysis so far focus on orth-MBenes, while the catalytic performances of hex-MBenes are also highly expected. Overall, further explorations on the catalytic properties for MBenes are needed, and comprehensive considerations of the above issues would make the study of catalysis closer to practical applications.

Primary achievements have been made in the field of MBenes. To step in the next stage, there are many other areas to be explored. Firstly, new-type MBenes remain to be discovered. As discussed above, orth-M_2B_2 and hex-M_2B_2 are the most common MBenes so far, with few orth/hex-M_3B_4 and orth-M_4B_6 being available. Therefore, exploring new $M_{n+1}B_{2n}$-type MBenes with $n > 1$ would be an important and interesting topic in MBenes. Besides the normal binary MBenes with perfect crystal lattices, other derived MBenes with different structures and compositions have been studied preliminarily. Very recently, a series of quaternary hexagonal 3D double-TM MAB phases with in-plane chemical ordering (named i-MAB) were predicted and $Mo_{4/3}Y_{2/3}AlB_2$ and $Mo_{4/3}Sc_{2/3}AlB_2$ were synthesized.[47,48] By HF-etching, both Al and Y/Sc atoms along with a small amount of B atoms were removed and hexagonal 2D $Mo_{4/3}B_{2-x}$ was obtained, which possesses in-plane ordered Mo vacancies.[46] This indicated that both the light TM atoms and Al atoms could be etched out from i-MAB phases to obtain binary hex-MBenes with ordered vacancies. Besides $Mo_{4/3}Y_{2/3}AlB_2$ and $Mo_{4/3}Sc_{2/3}AlB_2$, there are also many other i-MAB phases that were proved to be stable.[47,48] Thus, $M_{4/3}B_2$ (M = Ti, Cr, Mn, Fe, W) hex-MBenes are expected to be obtained if their precursors are available. Meanwhile, it has been predicted that double-metal hex-MBenes, $M'_{1/3}M''_{2/3}B_2$, could exist theoretically by removing the A atomic layers in i-MAB phases.[47] In addition, solid solution quaternary orth-MAB phases, $Fe_{2-x}Mn_xAlB_2$,[78] and quaternary orth-MAB phases with out-of-plane ordering, $M_2M'AlB_4$ phases (M = Mn, Fe, Co and M′ = Cr, Mo, W),[79] have been synthesized and predicted, respectively. Therefore, solid solutions $Fe_{2-x}Mn_xB_2$ and ordered orth-$M_2M'B_4$ are also possible to be obtained. Possessing complex composition and defects in structures, these MBenes would exhibit unique properties, which deserve further investigations.

As discussed above, synthesis is one of the critical constraints for MBene development, and therefore deserves more attentions in the future. The breakthrough could be made from two aspects: precursors and synthetic methods. By far, only three MAB phases have been applied as precursors for corresponding MBenes experimentally. Besides Cr_2AlB_2, MoAlB orth-MAB and Ti_2InB_2 hex-MAB phases, there are Cr_3AlB_4, Cr_4AlB_6, Mn_2AlB_2, Fe_2AlB_2 and WAlB orth-MAB available. Therefore, Cr_3B_4, Cr_4B_6, Mn_2B_2, Fe_2B_2 and W_2B_2 are expected to be obtained and should be considered for experimental preparation. In the synthesis of MBenes, the bond nature of MAB phases plays a pivotal role and thus relevant in-depth research both theoretically and experimentally is in urgent need and strongly encouraged. On the other hand, synthetic methods for MBenes are much fewer than those for MXenes, which is also one critical reason that fewer MBenes are available than MXenes. Since MAB phases possess such similar bond nature to MAX phases, many other synthetic methods applied for MXenes are worthy to be attempted, such as difluoride salt etching, molten salt etching, electrochemical etching, and bottom-up approaches.[11]

So far, MBenes have been mostly used for research of energy storage and catalysis, in which they have shown innate advantages. Firstly, pristine MBenes are all metallic, which would contribute to higher charge transfer efficiency as either electrodes or electrocatalysts than some semiconductive 2D materials such as MoS_2,[4] $Ti_3C_2O_2$ (ref. 70) and h-BN.[3] Besides, in contrast to MXenes, the surfaces of MBenes seem to be less easily terminated during the synthesis process, especially in acid solutions,[11] which makes their surface composition more controllable. Therefore, MBenes could provide stronger binding force to ions and molecules than terminated-MXenes[70] and TMDs[4] in aqueous solutions, which is conducive for some electrocatalytic reactions.

Furthermore, the applications of MBenes should be broadened other than energy storage and electrocatalysis. On the one hand, MBenes possess similar compositions and structures to MXenes, and the applications of MXenes could be taken as reference. For example, photocatalysis, electronic devices, sensors or biochemistry could be potential applications for MBenes. On the other hand, compared with MXenes, the MBene family contains more members with late-transition metals, including Fe, Mn, and Cr, all of which are magnetic systems. Therefore, the utilization of magnetism of MBenes would be an intriguing and distinctive application direction.

Significantly, one of the characteristics of MBenes different from MXenes is that there exist two phases for some systems, including orthorhombic and hexagonal Sc_2B_2, Y_2B_2, Ti_2B_2, Zr_2B_2, Hf_2B_2, V_2B_2, Nb_2B_2, Ta_2B_2, Cr_2B_2, Mo_2B_2 and W_2B_2, all of which are early transition metal-based MBenes. Therefore, a comparative study of hex-MBenes, orth-MBenes and MXenes with the same transition metal element would be an intriguing topic. Moreover, the in-depth mechanism of phase changes between orthorhombic and hexagonal phases is also worth of

further investigations from both the theoretical and experimental perspectives.

In summary, as a new family of 2D materials, MBenes have exhibited many attractive properties and promising applications for energy storage and electrocatalysis. Meanwhile, there exist great potential and some obstacles in this field. We hope this work would present a comprehensive and clear introduction of MBenes and inspire more researchers to focus on this field and explore the future of MBenes.

Conflicts of interest

There are no conflicts to declare.

Acknowledgements

This work was financially supported by the National Natural Science Foundation of China (No. 51871009 and 51872017).

References

1 K. S. Novoselov, A. K. Geim, S. V. Morozov, D. Jiang, Y. Zhang, S. V. Dubonos, I. V. Grigorieva and A. A. Firsov, *Science*, 2004, **306**, 666.
2 H. Zhang, *ACS Nano*, 2015, **9**, 9451–9469.
3 Y. Lin, T. V. Williams and J. W. Connell, *J. Phys. Chem. Lett.*, 2010, **1**, 277–283.
4 M. Chhowalla, H. S. Shin, G. Eda, L.-J. Li, K. P. Loh and H. Zhang, *Nat. Chem.*, 2013, **5**, 263–275.
5 Q. Wang and D. O'Hare, *Chem. Rev.*, 2012, **112**, 4124–4155.
6 H. Liu, Y. Du, Y. Deng and P. D. Ye, *Chem. Soc. Rev.*, 2015, **44**, 2732–2743.
7 M. Naguib, M. Kurtoglu, V. Presser, J. Lu, J. Niu, M. Heon, L. Hultman, Y. Gogotsi and M. W. Barsoum, *Adv. Mater.*, 2011, **23**, 4248–4253.
8 Z. Guo, J. Zhou and Z. Sun, *J. Mater. Chem. A*, 2017, **5**, 23530–23535.
9 H. Zhang, H. Xiang, F.-z. Dai, Z. Zhang and Y. Zhou, *J. Mater. Sci. Technol.*, 2018, **34**, 2022–2026.
10 L. T. Alameda, P. Moradifar, Z. P. Metzger, N. Alem and R. E. Schaak, *J. Am. Chem. Soc.*, 2018, **140**, 8833–8840.
11 Y. Wei, P. Zhang, R. A. Soomro, Q. Zhu and B. Xu, *Adv. Mater.*, 2021, **33**, 2103148.
12 M. Li, J. Lu, K. Luo, Y. Li, K. Chang, K. Chen, J. Zhou, J. Rosen, L. Hultman, P. Eklund, P. O. Å. Persson, S. Du, Z. Chai, Z. Huang and Q. Huang, *J. Am. Chem. Soc.*, 2019, **141**, 4730–4737.
13 B. Anasori, M. R. Lukatskaya and Y. Gogotsi, *Nat. Rev. Mater.*, 2017, **2**, 16098.
14 M. D. Levi, M. R. Lukatskaya, S. Sigalov, M. Beidaghi, N. Shpigel, L. Daikhin, D. Aurbach, M. W. Barsoum and Y. Gogotsi, *Adv. Energy Mater.*, 2015, **5**, 1400815.
15 N. Sun, Q. Zhu, B. Anasori, P. Zhang, H. Liu, Y. Gogotsi and B. Xu, *Adv. Funct. Mater.*, 2019, **29**, 1906282.
16 M. R. Lukatskaya, O. Mashtalir, C. E. Ren, Y. Dall'Agnese, P. Rozier, P. L. Taberna, M. Naguib, P. Simon, M. W. Barsoum and Y. Gogotsi, *Science*, 2013, **341**, 1502–1505.
17 Z. Guo, N. Miao, J. Zhou, B. Sa and Z. Sun, *J. Mater. Chem. C*, 2017, **5**, 978–984.
18 K. Hantanasirisakul and Y. Gogotsi, *Adv. Mater.*, 2018, **30**, 1804779.
19 G. Gao, A. P. O'Mullane and A. Du, *ACS Catal.*, 2017, **7**, 494–500.
20 Z. Guo, J. Zhou, L. Zhu and Z. Sun, *J. Mater. Chem. A*, 2016, **4**, 11446–11452.
21 J. Peng, X. Chen, W.-J. Ong, X. Zhao and N. Li, *Chem*, 2019, **5**, 18–50.
22 J. Zhang, Y. Zhao, X. Guo, C. Chen, C.-L. Dong, R.-S. Liu, C.-P. Han, Y. Li, Y. Gogotsi and G. Wang, *Nat. Catal.*, 2018, **1**, 985–992.
23 S. Chertopalov and V. N. Mochalin, *ACS Nano*, 2018, **12**, 6109–6116.
24 X. Zhan, C. Si, J. Zhou and Z. Sun, *Nanoscale Horiz.*, 2020, **5**, 235–258.
25 R. Li, Z. Liu, Q. T. Trinh, Z. Miao, S. Chen, K. Qian, R. J. Wong, S. Xi, Y. Yan, A. Borgna, S. Liang, T. Wei, Y. Dai, P. Wang, Y. Tang, X. Yan, T. S. Choksi and W. Liu, *Adv. Mater.*, 2021, **33**, 2101536.
26 Q. Yu, Y. Fang, X. Cao, S. Wu and Z.-z. Zhu, *Appl. Phys. Lett.*, 2021, **118**, 183101.
27 I. Ozdemir, Y. Kadioglu, O. Üzengi Aktürk, Y. Yuksel, Ü. Akıncı and E. Aktürk, *J. Phys.: Condens. Matter*, 2019, **31**, 505401.
28 Y. Zuntu Abdullahi, Z. Demir Vatansever, E. Aktürk, Ü. Akıncı and O. Üzengi Aktürk, *Phys. Chem. Chem. Phys.*, 2020, **22**, 10893–10899.
29 M. Ade and H. Hillebrecht, *Inorg. Chem.*, 2015, **54**, 6122–6135.
30 F. Li and Q. Tang, *ACS Appl. Nano Mater.*, 2019, **2**, 7220–7229.
31 X. Guo, S. Lin, J. Gu, S. Zhang, Z. Chen and S. Huang, *Adv. Funct. Mater.*, 2021, **31**, 2008056.
32 S. Qi, Y. Fan, L. Zhao, W. Li and M. Zhao, *Appl. Surf. Sci.*, 2021, **536**, 147742.
33 Y. Xiao, C. Shen and T. Long, *Chem. Mater.*, 2021, **33**, 4023–4034.
34 Y. Xiao and C. Shen, *Small*, 2021, **17**, 2100776.
35 Y. Cheng, J. Mo, Y. Li, Y. Zhang and Y. Song, *Phys. Chem. Chem. Phys.*, 2021, **23**, 6613–6622.
36 B. Zhang, J. Zhou, Z. Guo, Q. Peng and Z. Sun, *Appl. Surf. Sci.*, 2020, **500**, 144248.
37 M. Jakubczak, A. Szuplewska, A. Rozmysłowska-Wojciechowska, A. Rosenkranz and A. M. Jastrzębska, *Adv. Funct. Mater.*, 2021, **31**, 2103048.
38 Z. Jiang, P. Wang, X. Jiang and J. Zhao, *Nanoscale Horiz.*, 2018, **3**, 335–341.
39 X. Liu, X. Ge, Y. Dong, K. Fu, F. Meng, R. Si, M. Zhang and X. Xu, *Mater. Chem. Phys.*, 2020, **253**, 123334.
40 T. Bo, P.-F. Liu, J. Xu, J. Zhang, Y. Chen, O. Eriksson, F. Wang and B.-T. Wang, *Phys. Chem. Chem. Phys.*, 2018, **20**, 22168–22178.
41 J. Wang, T.-N. Ye, Y. Gong, J. Wu, N. Miao, T. Tada and H. Hosono, *Nat. Commun.*, 2019, **10**, 2284.

42 N. Miao, J. Wang, Y. Gong, J. Wu, H. Niu, S. Wang, K. Li, A. R. Oganov, T. Tada and H. Hosono, *Chem. Mater.*, 2020, **32**, 6947–6957.
43 T. Gorkan, E. Vatansever, Ü. Akıncı, G. Gökoglu, E. Aktürk and S. Ciraci, *J. Phys. Chem. C*, 2020, **124**, 12816–12823.
44 K. Rasoul, K. Mohammad, W. Vei, M. Nanxi, S. Chen, W. Jianfeng and W. Junjie, *J. Phys.: Condens. Matter*, 2020, **33**, 15533.
45 S. Gao, J. Hao, X. Zhang, L. Li, C. Zhang, L. Wu, X. Ma, P. Lu and G. Liu, *Comput. Mater. Sci.*, 2021, **200**, 110776.
46 J. Zhou, J. Palisaitis, J. Halim, M. Dahlqvist, Q. Tao, I. Persson, L. Hultman, P. O. Å. Persson and J. Rosen, *Science*, 2021, **373**, 801–805.
47 Y. Yao, N. Miao, Y. Gong and J. Wang, *Nanoscale*, 2021, **13**, 13208–13214.
48 M. Dahlqvist, Q. Tao, J. Zhou, J. Palisaitis and J. Rosen, *J. Am. Chem. Soc.*, 2020, **142**, 18583–18591.
49 T. Zhao, S. Zhang, Y. Guo and Q. Wang, *Nanoscale*, 2016, **8**, 233–242.
50 Y. Yu, Z. Guo, Q. Peng, J. Zhou and Z. Sun, *J. Mater. Chem. A*, 2019, **7**, 12145–12153.
51 X.-H. Zha, P. Xu, Q. Huang, S. Du and R.-Q. Zhang, *Nanoscale Adv.*, 2020, **2**, 347–355.
52 G. Bhaskar, V. Gvozdetskyi, M. Batuk, K. M. Wiaderek, Y. Sun, R. Wang, C. Zhang, S. L. Carnahan, F. Wu, R. A. Ribeiro, S. L. Bud'ko, P. C. Canfield, W. Huang, A. J. Rossini, C. Wang, K. Ho, J. Hadermann and J. V. Zaikina, *J. Am. Chem. Soc.*, 2021, **143**, 4213–4223.
53 S. K. Das, A. Bedar, A. Kannan and K. Jasuja, *Sci. Rep.*, 2015, **5**, 10522.
54 X. Yang, C. Shang, S. Zhou and J. Zhao, *Nanoscale Horiz.*, 2020, **5**, 1106–1115.
55 R. Meshkian, M. Dahlqvist, J. Lu, B. Wickman, J. Halim, J. Thörnberg, Q. Tao, S. Li, S. Intikhab, J. Snyder, M. W. Barsoum, M. Yildizhan, J. Palisaitis, L. Hultman, P. O. Å. Persson and J. Rosen, *Adv. Mater.*, 2018, **30**, 1706409.
56 M. Dou, H. Li, Q. Yao, J. Wang, Y. Liu and F. Wu, *Phys. Chem. Chem. Phys.*, 2021, **23**, 10615–10620.
57 I. Ozdemir, Y. Kadioglu, Y. Yüksel, Ü. Akıncı, O. Ü. Aktürk, E. Aktürk and S. Ciraci, *Phys. Rev. B*, 2021, **103**, 144424.
58 B. Li, Y. Wu, N. Li, X. Chen, X. Zeng, Arramel, X. Zhao and J. Jiang, *ACS Appl. Mater. Interfaces*, 2020, **12**, 9261–9267.
59 T. Zhang, B. Zhang, Q. Peng, J. Zhou and Z. Sun, *J. Mater. Chem. A*, 2021, **9**, 433–441.
60 M. Yao, Z. Shi, P. Zhang, W.-J. Ong, J. Jiang, W.-Y. Ching and N. Li, *ACS Appl. Nano Mater.*, 2020, **3**, 9870–9879.
61 J. Wang, C. He, J. Huo, L. Fu and C. Zhao, *Adv. Theory Simul.*, 2021, **4**, 2100003.
62 S. Xu, G. Qin, Q. Jiang, Q. Cui, A. Du, C. Zhao and Q. Sun, *Int. J. Quantum Chem.*, 2021, **121**, e26548.
63 Y. Li, L. Li, R. Huang and Y. Wen, *Nanoscale*, 2021, **13**, 15002–15009.
64 X. Liu, Z. Liu and H. Deng, *J. Phys. Chem. C*, 2021, **125**, 19183–19189.
65 Y. Xiao, C. Shen and N. Hadaeghi, *J. Phys. Chem. Lett.*, 2021, **12**, 6370–6382.
66 C. He, J. Wang, L. Fu, C. Zhao and J. Huo, *Chin. Chem. Lett.*, 2022, **33**, 1051–1057.
67 X. Zhu, X. Zhou, Y. Jing and Y. Li, *Nat. Commun.*, 2021, **12**, 4080.
68 M. Li, J. Lu, Z. Chen and K. Amine, *Adv. Mater.*, 2018, **30**, 1800561.
69 J. Jia, B. Li, S. Duan, Z. Cui and H. Gao, *Nanoscale*, 2019, **11**, 20307–20314.
70 Q. Tang, Z. Zhou and P. Shen, *J. Am. Chem. Soc.*, 2012, **134**, 16909–16916.
71 Z. Ma, F. Sun, M. Dou, Q. Yao, Y. Liu and F. Wu, *Phys. Lett. A*, 2020, **384**, 126282.
72 R. Li, Y. Liu, H. Deng, C. Yu and Z. Liu, *J. Electrochem. Energy Convers. Storage*, 2020, **17**, 041002.
73 K. Liu, B. Zhang, X. Chen, Y. Huang, P. Zhang, D. Zhou, H. Du and B. Xiao, *J. Phys. Chem. C*, 2021, **125**, 18098–18107.
74 Y. Xiao, Y. Li, Z. Guo, C. Tang, B. Sa, N. Miao, J. Zhou and Z. Sun, *Appl. Surf. Sci.*, 2021, **566**, 150634.
75 J. Long, S. Chen, Y. Zhang, C. Guo, X. Fu, D. Deng and J. Xiao, *Angew. Chem., Int. Ed.*, 2020, **59**, 9711–9718.
76 T. Li, L. Yao, Q. Liu, J. Gu, R. Luo, J. Li, X. Yan, W. Wang, P. Liu, B. Chen, W. Zhang, W. Abbas, R. Naz and D. Zhang, *Angew. Chem., Int. Ed.*, 2018, **57**, 6115–6119.
77 M. Cococcioni and S. de Gironcoli, *Phys. Rev. B: Condens. Matter Mater. Phys.*, 2005, **71**, 035105.
78 P. Chai, S. A. Stoian, X. Tan, P. A. Dube and M. Shatruk, *J. Solid State Chem.*, 2015, **224**, 52–61.
79 F.-Z. Dai, H. Xiang, Y. Sun and Y. Zhou, *J. Mater. Sci. Technol.*, 2019, **35**, 1432–1438.

